Instabilities and patterns in horizontally oscillating particulate suspension

Meheboob Alam*
Engineering Mechanics Unit and Max-Planck Partner Group, Jawaharlal Nehru Center for Advanced Scientific Research, Jakkur P. O., Bangalore 560064, India

Arzhang Khalili
Max Planck Institute for Marine Microbiology, 28359 Bremen, Germany
and Jacobs University Bremen, 28759 Bremen, Germany
(Received 14 January 2008; published 9 April 2008)

The mean flow and the linear stability characteristics of a two-dimensional particulate suspension, driven horizontally via harmonic oscillation, are analyzed. A constitutive model based on the kinetic theory of granular materials, which takes into account the dissipative collisional interactions among particles as well as their interactions with the interstitial fluid, is used; the effects of the interstitial fluid are incorporated in the balance equations for the particle phase. Assuming that the suspension is thin along the vertical direction, the effects of driving are incorporated into the governing equations in a mean-field manner. Using Floquet theory, a linear stability analysis of the time-periodic mean flow indicates that the oscillatory suspension supports stationary- and traveling-wave instabilities which correspond to particle banding patterns that are aligned parallel or orthogonal or at an oblique angle to the driving direction. The effects of external driving parameters and various system control parameters on the phase diagram of instabilities are studied. The fluid-particle interaction is shown to be responsible for the emergence of traveling instabilities in this flow.

DOI: 10.1103/PhysRevE.77.041305 PACS number(s): 45.70.Qj, 47.11.−j, 47.20.Ma, 89.75.Da

I. INTRODUCTION

Granular materials, collections of macroscopic particles, are ubiquitous in our daily lives and industrial processes. There exist close analogies between dry granular flows and liquid flows [1,2]. For example, recent experiments [3] have confirmed that the patterns in Martian gullies can be reproduced by performing experiments with dry granular materials. However, the presence of interstitial fluid significantly complicates the dynamics of granular materials. Hydrodynamic interactions lead to viscous drag and anisotropic long-range interactions among particles [4] which are responsible for the emergence of patterns in many flows. The fluid-particle interaction also plays an important role in many geophysical problems such as sedimentation, erosion, and wind- and water-driven granular flows. The former is the cause of dune and shore-line formation as well as their migration [5–8]. In the case of water currents over flat sand beds, the ripples are seen to form if the flow rate exceeds a certain threshold value [5,9]. Such underwater sand ripples also form due to oscillatory flows, which are induced by the surface waves in shallow water [10–13]. One of the most technologically important examples of particle-laden flows is a fluidized bed. A uniform fluidization, the most desirable regime for most industrial applications [14], turns out to be prone to bubbling instability. Instabilities in fluidized beds belong to an active area of research in the engineering community [14]. Recently, there have been a series of experiments [15] to unveil the important role of air in various types of granular flows. In this regard, one can try to understand the role of air by incorporating the effect of air in a mean-field manner into the standard continuum equations for dry granular flows.

To make progress in understanding the mechanisms responsible for pattern formation in a driven particle-fluid mixture, one needs to understand the physics of fluid-particle interactions from the viewpoint of predicting dynamical features in particulate suspensions using macroscopic balance equations. It would be worthwhile to investigate the flow and stability characteristics of a fluid-particle mixture via linear stability analysis. As a first step toward this goal, we have focused on a model problem of a harmonically driven particle-fluid mixture. The suspension is shaken horizontally via a sinusoidal vibrator, representing a bulk forcing of the suspension, i.e., the energy is pumped into the system uniformly. Since there are many unsettled issues regarding boundary conditions in particulate flows [2], we assume that the suspension is of infinite extent (in the horizontal plane), and the effects of the oscillating bottom plate are incorporated into the governing equations in a mean-field manner. The goal is to probe and understand the possible pattern formation scenario in such a simple setup. It may be pointed out that there are many linear stability works (see [2,4] for reviews) on particulate flows with *steady base states*; however, the present effort is directed toward analyzing instabilities in a *time-dependent* base state.

Drawing an analogy with recent works on rapid granular flows [2,16] and suspensions [17,18], an effective continuum model for a suspension of particle-fluid mixture is outlined in Sec. II. Along with the standard mass and momentum balance equations for the particle phase, we consider an additional balance equation for the fluctuation kinetic energy of the particles. The effects of fluid are taken into account in the momentum equation for the particle phase as well as in the fluctuation energy equation. Based on this coarse-grained model, we analyze the mean flow and the linear stability

*Corresponding author. meheboob@jncasr.ac.in

characteristics of a harmonically driven suspension. The onset of instabilities is tied to the emergence of bandlike patterns of particles that are aligned parallel and/or orthogonal to the driving direction. The phase diagram for instabilities is studied as a function of external driving parameters and various system parameters. We close by discussing the limitations of the present hydrodynamic model.

II. GOVERNING EQUATIONS FOR PARTICULATE SUSPENSION

As mentioned before, the governing equations are motivated by the theories of dry granular flows [2] which have been successful in explaining pattern formations in different prototypical flows [2,4]. We assume that the particle-fluid mixture can be modeled as an effective continuum of the particle phase, and the effect of fluid is taken into account via certain interaction terms in the balance equations for the particle phase.

The balance equations for the mass, momentum, and fluctuation energy of the particle phase are

$$\left(\frac{\partial}{\partial t}+\mathbf{u}\cdot\boldsymbol{\nabla}\right)\rho=-\rho\,\boldsymbol{\nabla}\cdot\mathbf{u}, \tag{1}$$

$$\rho\left(\frac{\partial}{\partial t}+\mathbf{u}\cdot\boldsymbol{\nabla}\right)\mathbf{u}=-\boldsymbol{\nabla}\cdot\Sigma+\rho\mathbf{g}+\mathbf{F}_d, \tag{2}$$

$$\frac{\dim}{2}\rho\left(\frac{\partial}{\partial t}+\mathbf{u}\cdot\boldsymbol{\nabla}\right)T=-\boldsymbol{\nabla}\cdot\mathbf{q}-\Sigma:\boldsymbol{\nabla}\mathbf{u}+E-\mathcal{D}-\mathcal{D}_v, \tag{3}$$

respectively. Here $\rho=\rho_p\phi$ is the mass density of particles, with ρ_p being the material density of particles and ϕ their volume fraction (i.e., the fraction of volume occupied by the particles); $\mathbf{u}=\langle\mathbf{c}\rangle$ is the "macroscopic" velocity of the particles where $\mathbf{c}$ is the instantaneous particle velocity; $T=\langle(\mathbf{c}-\mathbf{u})^2/\dim\rangle$ is the mean square of the fluctuation velocity of particles (i.e., the fluctuation kinetic energy of particles or the pseudothermal energy), commonly known as the "granular" temperature; dim is the dimension. A separate balance equation for T is needed since the transport coefficients depend on T. In the momentum balance equation, g is the gravitational acceleration, $\mathbf{F}_d$ the drag force due to interstitial fluid, and Σ the stress tensor for the particle phase. In the energy balance equation, the first term on the right-hand side $\boldsymbol{\nabla}\cdot\mathbf{q}$ represents the flux of pseudothermal energy, the second term $\Sigma:\boldsymbol{\nabla}\mathbf{u}$ the shear work, the third term E the total source of fluctuation energy due to the hydrodynamic interaction and bulk forcing, the fourth term $\mathcal{D}$ the loss of fluctuation energy due to the inelastic nature of particle collisions, and the last term $\mathcal{D}_v$ the loss of fluctuation energy due to viscous dissipation of the interstitial fluid. Note that $E=E_h+E_s$ where E_h represents the source of fluctuation energy due to the hydrodynamic interaction between the fluid and the particle phase, and E_s the source of energy due to bulk excitation (as detailed in Sec. III A).

In the present model, the particle-fluid mixture is modeled by the single-phase equations for dry granular flows, and the effects of interstitial fluid phase are taken into account via three terms: (1) the drag force $\mathbf{F}_d$ in the momentum equation, (2) the viscous dissipation $\mathcal{D}_v$, and (3) the hydrodynamic source of energy E_h in the fluctuation energy equation. Since $\mathbf{F}_d$ and E_h depend on the *slippage* (see Sec. II A 2) between the macroscopic velocity of the particle phase and the fluid velocity, the fluid velocity field (or the slippage velocity) needs to be specified *a priori*.

It should be noted that the basis of the effective single-phase description of a particle-fluid mixture hinges on the assumption that the coupling between two phases is weak. This assumption of weak coupling is strictly valid in the limit of large Stokes number (the ratio between the particle relaxation time and the external time scale), and hence this model is more appropriate for a gas-particle suspension (see Sec. III B for details). However, we believe that many dynamical features of a high-Stokes-number particulate suspension carry over to those of a low-Stokes-number suspension too [19].

A. Constitutive model

1. Constitutive model for the particle phase

Here we use the theory of Lun *et al.* [16] as the constitutive model for the particle phase; this model as well as its variants have been extensively used to investigate various canonical problems in rapid granular flows [2].

The stress tensor and the heat flux for the particle phase can be written as

$$\Sigma=[p-\zeta(\boldsymbol{\nabla}\cdot\mathbf{u})]\mathbf{I}-2\mu\mathbf{S}, \tag{4}$$

$$\mathbf{q}=-\kappa\,\boldsymbol{\nabla}T, \tag{5}$$

respectively, where p is the pressure, μ the shear viscosity, ζ the bulk viscosity, and κ the pseudothermal conductivity of the particle assembly, $\mathbf{S}$ is the deviatoric strain rate tensor, and $\mathbf{I}$ is the unit tensor. The expressions for p, μ, ζ, κ, and the collisional dissipation $\mathcal{D}$ are given by

$$p=\rho_p T f_1(\phi),\quad (\mu,\zeta)=\rho_p d T^{1/2}[f_2(\phi),f_3(\phi)], \tag{6}$$

$$\kappa=\rho_p d T^{1/2} f_4(\phi),\quad \mathcal{D}=\frac{\rho_p}{d}T^{3/2}f_5(\phi), \tag{7}$$

respectively, where d is the particle diameter, and the f_i's are nondimensional functions of particle volume fraction that are taken to be those for a dense system of hard spheres [16]:

$$f_1(\phi)=\phi(1+4\phi\chi),$$

$$f_2(\phi)=\frac{5\sqrt{\pi}}{96\chi}\left(1+\frac{8}{5}\phi\chi\right)^2+\frac{8}{5\sqrt{\pi}}\phi^2\chi,$$

$$f_3(\phi)=\frac{8}{3\sqrt{\pi}}\phi^2\chi,$$

$$f_4(\phi)=\frac{25\sqrt{\pi}}{128\chi}\left(1+\frac{12}{5}\phi\chi\right)^2+\frac{4}{\sqrt{\pi}}\phi^2\chi,$$

$$f_5(\phi) = \frac{12}{\sqrt{\pi}}(1-e^2)\phi^2\chi. \tag{8}$$

Here, $\chi(\phi)$ is the contact radial distribution function, which is taken to be of the following form [20]:

$$\chi(\phi) = \frac{1+2.5\phi+5.0\phi^2+4.5\phi^3}{[1-(\phi/\phi_{\max})^3]^{2/3}}. \tag{9}$$

This expression agrees with the Carnahan-Starling function almost perfectly up to a particle volume fraction of $\phi=0.5$ and diverges at the random close packing limit ($\phi_{\max}=0.65$).

2. Coupling with fluid

The constitutive model for the coupling terms in the particle-phase balance equations is adapted from the theory of Sangani *et al.* [18]. In the following we briefly outline different terms and the reader is referred to the original paper for further details.

The constitutive expression for the drag force for a system of monodisperse particles is taken to be of the form

$$\mathbf{F}_d = \frac{\rho_p}{\tau_r}(\mathbf{u}_f - \mathbf{u})f_6(\phi) \tag{10}$$

where

$$\mathbf{u_f} - \mathbf{u} \equiv \mathbf{U} \tag{11}$$

is the slippage velocity between fluid and particle phases, τ_r is the relaxation time of a particle,

$$\tau_r = \frac{m}{3\pi d\mu_f}, \tag{12}$$

with μ_f being the shear viscosity of the interstitial fluid, and the nondimensional function f_6 is [21]

$$f_6(\phi) = \phi R_d(\phi)$$

with

$$R_d(\phi) = \frac{10\phi}{(1-\phi)^3} + (1+1.5\phi^{1/2})(1-\phi). \tag{13}$$

Note that the first term in Eq. (13) represents the well-known Carman-Kozeny correlation for a dense suspension. This expression for the drag function $R_d(\phi)$ is assumed to be valid for the whole range of volume fractions under homogeneous flow as confirmed recently via lattice Boltzmann simulations [21], and differs from the one suggested by Sangani *et al.* [18], which is valid for $\phi<0.4$. The drag function is directly related to the permeability of the two-phase medium for which an equation was derived by Brinkman [22] that is valid for a dilute suspension. Brinkman's formula was subsequently improved by Kim and Russel [23] for the whole range of particle volume fractions using asymptotic expansions of pertinent governing equations.

The rate of viscous dissipation per unit volume due to the presence of the interstitial fluid is [18]:

$$\mathcal{D}_v = \frac{\rho_p}{\tau_r} T f_{5v}(\phi), \tag{14}$$

where

$$f_{5v}(\phi) = 3\phi\left(1 + \frac{3\sqrt{\phi}}{\sqrt{2}} + \frac{135}{64}\phi\ln\phi + 11.26\phi(1-5.1\phi + 16.57\phi^2 - 21.77\phi^3) - \phi\chi\ln\epsilon_m\right), \tag{15}$$

where ϵ_m is the lubrication cutoff scale [18], which is proportional to the ratio between the mean free path of the fluid molecules and the particle diameter. The related viscous dissipation function [18] $R_{\text{diss}}=f_{5v}/3\phi$ can be thought of as an effective drag coefficient of a sphere which is moving through a fixed bed of particles in the presence of a mean flow [23]. It can be verified [18] that R_{diss} agrees with the drag function [R_d in Eq. (13)] up to the terms of $O(\phi\ln\phi)$, and the higher-order terms in Eq. (15) have been obtained by curve-fitting the particle simulation results as discussed by Sangani *et al.* The above constitutive expression (15) has been verified [18] to hold up to a particle volume fraction of $\phi=0.4$.

The slippage between the fluid and the particle phase is responsible for the generation of fluctuating kinetic energy [18]:

$$E_h = \frac{\rho_p d}{\tau_r^2 T^{1/2}} U^2 f_{7h}(\phi), \tag{16}$$

where $\mathbf{U}=(\mathbf{u}_f-\mathbf{u})$ is the slippage velocity and

$$f_{7h}(\phi) = \frac{3}{16\sqrt{\pi}}\phi R_s R_d^2 \quad \text{and} \quad R_s = \frac{1}{\chi(1+3.5\sqrt{\phi}+5.9\phi)}. \tag{17}$$

III. OSCILLATORY SUSPENSION

Consider a collection of particles on a plate (immersed in a fluid), oscillated horizontally via a harmonic oscillation

$$x(t) = A\sin(\omega t), \tag{18}$$

where A is the amplitude of oscillation and $\omega=2\pi f$ is the angular frequency of oscillation; the particle-fluid suspension is assumed to be in a fluidized state via this "uniform" shaking. In this paper, we restrict ourselves to an effective two-dimensional suspension in the (x,y) plane of infinite extent, with a thin layer of particles along the vertical direction; here x is directed along the driving path and y is perpendicular to it on the same plane, as shown schematically in Fig. 1.

A. Boundary conditions: Effective terms

Here we outline how to incorporate boundary conditions at the oscillating plate. Note that the base plate is oscillating with a velocity $V_p(t)=A\omega\cos\omega t$ in the (x,y) plane. Since we are considering a thin layer of particles, we can disregard this velocity boundary condition at the plate but instead we as-

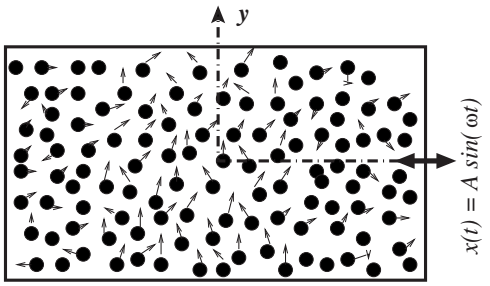

FIG. 1. Schematic of a suspension of particles of diameter d under horizontal oscillation. A is the oscillation amplitude and $\omega = 2\pi f$ is the angular frequency of oscillation.

sume that the suspension is subjected to an accelerating force

$$F_a(t) = \rho \frac{dV_p}{dt} = -\rho_p \phi A \omega^2 \sin \omega t \tag{19}$$

along the driving direction.

Within the thin-layer approximation, our suspension is two dimensional [in the horizontal (x,y) plane], and disregarding the boundary conditions at the plate is equivalent to adding two terms in the governing equations: (i) an accelerating force F_a in the x momentum equation, and (ii) an energy source term E_s in the granular energy equation, which is calculated in Sec. III A 1. While the first term is equivalent to specifying the velocity boundary condition, the latter term is equivalent to specifying a boundary condition on the granular temperature at the plate.

1. Energy source due to uniform excitation

Here we estimate the amount of fluctuation energy that is being pumped into the system via the shaker in terms of the oscillation parameters (A and ω) and the suspension parameters (ϕ and T). For sinusoidal shaking, the mean velocity is zero but the mean square of the plate velocity is

$$\langle V_p^2 \rangle = \frac{1}{\tau}\int_0^\tau V_p^2(t)dt = \frac{1}{\tau}\int_0^\tau A^2\omega^2 \cos^2 \omega t \, dt = \frac{A^2\omega^2}{2},$$

where $\tau = 2\pi/\omega$ is the period of oscillation. Assuming that the suspension is uniformly shaken, the average shear rate across a layer of height h is given by

$$\frac{\sqrt{\langle V_p^2 \rangle}}{h} = \frac{A\omega}{\sqrt{2}h},$$

and hence the shear stress experienced by the suspension is

$$S = \mu \times (\text{average shear rate}) = \mu\left(\frac{A\omega}{\sqrt{2}h}\right),$$

where μ is the shear viscosity of the particle phase, which can be taken as that discussed in Sec. II A 1. Assuming that the suspension is characterized by a constant granular temperature T, an expression for the input fluctuation energy E_s (energy input per unit volume per unit time) is given by the product of the shear stress and the average shear rate:

$$E_s = S \times (\text{average shear rate})$$
$$= \mu\frac{A^2\omega^2}{2h^2} = \rho_p\left(\frac{d}{h^2}\right) f_7(\phi)\sqrt{T}A^2\omega^2, \tag{20}$$

with f_7 being a nondimensional function of particle volume fraction,

$$f_7(\phi) = \frac{1}{2} f_2(\phi). \tag{21}$$

It must be noted that the above expression of E_s remains valid as long as the suspension is uniformly shaken across its height, which amounts to negligible inhomogeneity due to gravitational compaction, which is the case if the suspension is thin along the vertical direction. Heretofore, focusing on a monolayer of suspension, we set $h=d$ in Eq. (20).

B. Mean flow: Granular temperature and particle velocity

Since the suspension is of infinite extent in both x and y directions, we can make the following assumptions on the mean flow (base-state) quantities: $\phi(\mathbf{x},t)$, $\mathbf{u}(\mathbf{x},t)$, and $T(\mathbf{x},t)$ are spatially homogeneous, i.e., $\nabla(\phi,\mathbf{u},T)=\mathbf{0}$.

It follows from the mass balance equation that $\partial\phi/\partial t = 0$, i.e., the particle volume fraction ϕ is time independent. The granular temperature is, however, time dependent which is governed by

$$\rho_p \phi \frac{dT}{dt} = E - \mathcal{D} - \mathcal{D}_v. \tag{22}$$

It has been verified that the source of granular energy due to hydrodynamic interactions, E_h, is small compared to that supplied via the uniform oscillation

$$E_h \ll E_s,$$

if the slippage between the particle and fluid velocities is small and/or if the Stokes number

$$\mathrm{St} = \omega\tau_r \tag{23}$$

is large; hence $E = E_s + E_h \approx E_s$. Using $t_R = \omega^{-1}$ and $T_R = d^2\omega^2$ as the reference time and temperature, respectively, the dimensionless granular energy equation simplifies to

$$\phi\frac{dT^*}{dt} = -f_5\left[T^* + \mathrm{St}^{-1}\frac{f_{5v}}{f_5}\sqrt{T^*} - \left(\frac{A}{d}\right)^2\frac{f_7}{f_5}\right]\sqrt{T^*}, \tag{24}$$

where $T^* := T/d^2\omega^2$ is the nondimensional granular temperature. This equation has an exact solution,

$$\sqrt{T^*(t)} = \frac{1}{2}(\beta_1+\beta_2) + \frac{1}{2}(\beta_1-\beta_2)\left(\frac{1+(\beta_1/\beta_2)e^{-\alpha t}}{1-(\beta_1/\beta_2)e^{-\alpha t}}\right), \tag{25}$$

where

$$\beta_1 = \frac{1}{2\,\mathrm{St}}\frac{f_{5v}}{f_5}\left(-1+\sqrt{1+4(A/d)^2\mathrm{St}^2\frac{f_5 f_7}{f_{5v}^2}}\right) > 0,$$

$$\beta_2 = \frac{1}{2\,\mathrm{St}}\frac{f_{5v}}{f_5}\left(-1-\sqrt{1+4(A/d)^2\mathrm{St}^2\frac{f_5 f_7}{f_{5v}^2}}\right) < 0,$$

$$\alpha = \frac{f_{5v}}{2\phi\ \mathrm{St}}\sqrt{1+4(A/d)^2\mathrm{St}^2\frac{f_5 f_7}{f_{5v}^2}} > 0.$$

In the asymptotic time limit ($t\to\infty$), this unsteady temperature field relaxes to a steady value:

$$T^{*1/2}(t\to\infty)\to\beta_1 = \frac{1}{2\ \mathrm{St}}\frac{f_{5v}}{f_5}\left(-1+\sqrt{1+4(A/d)^2\mathrm{St}^2\frac{f_5 f_7}{f_{5v}^2}}\right). \tag{26}$$

For the stability analysis in Sec. IV, we use this relaxed, steady temperature field as the base state.

It is clear that the steady, spatially uniform granular temperature can be obtained simply from a balance between the input energy from the shaker and the net dissipation due to the inelastic collision of particles and the viscous interaction due to the interstitial fluid:

$$E = \mathcal{D} + \mathcal{D}_v. \tag{27}$$

In the limit of large Stokes number ($\mathrm{St}\gg 1$), the collisional dissipation dominates over the viscous dissipation:

$$\mathcal{D} \gg \mathcal{D}_v \quad \text{as} \quad \mathrm{St}\to\infty,$$

which corresponds to the limit of rapid flows of dry granular materials for which the interaction with the interstitial fluid can be neglected. Equating the power input with the inelastic dissipation ($E=\mathcal{D}$), we obtain

$$T = \frac{f_7}{f_5}\left(\frac{A}{d}\right)^2 d^2\omega^2 \equiv T_{\mathrm{inel}}. \tag{28}$$

On the other hand, for particles with perfectly elastic collisions, the collisional dissipation is identically zero. Hence, in this limit the input energy is balanced by the viscous dissipation ($E=\mathcal{D}_v$), leading to

$$T = \mathrm{St}^2\left(\frac{A}{d}\right)^4\frac{f_7^2}{f_{5v}^2}d^2\omega^2 \equiv T_{\mathrm{vis}}. \tag{29}$$

One of these two limiting solutions (28) and (29) provides an upper bound on the steady granular temperature T, depending on the relative dominance of viscous dissipation over inelastic dissipation, and vice versa. For the general case, we have a quadratic equation for $\sqrt{T}$ having a positive solution, given by Eq. (26).

Figure 2 displays the variation of the steady granular temperature $T/d^2\omega^2$ with particle volume fraction (ϕ) for different oscillation frequencies. The amplitude of oscillation is set to $A/d=2$, with other parameters $e=0.9$, $d=1.0$ mm, and $\rho_p=2.5$ gm/cm^3. (With increasing A/d, T increases, with other parameters being fixed.) The properties of the interstitial fluid are taken to be those of air and water, respectively, in Figs. 2(a) and 2(b). For a given oscillation strength, the granular temperature decreases sharply with increasing ϕ and reaches a plateau in the dense limit. Comparing Figs. 2(a) and 2(b), we find that for the same driving and the particle parameters the granular temperature is lower in water than that in air. Since the particle relaxation time is inversely proportional to the fluid viscosity, the larger the viscosity the smaller the Stokes number, leading to a lower granular temperature in water. With parameter values as in Fig. 2, the Stokes numbers for a gas-particle suspension are 46.9 and 469.1 at $f=1$ and 10 Hz, respectively; the corresponding Stokes numbers for a water-particle suspension are 1.1 and 10.9, respectively, Since the adopted constitutive model is valid in the limit of large Stokes number for which the coupling between the fluid and particles is weak, our results are, therefore, more appropriate for a gas-particle suspension.

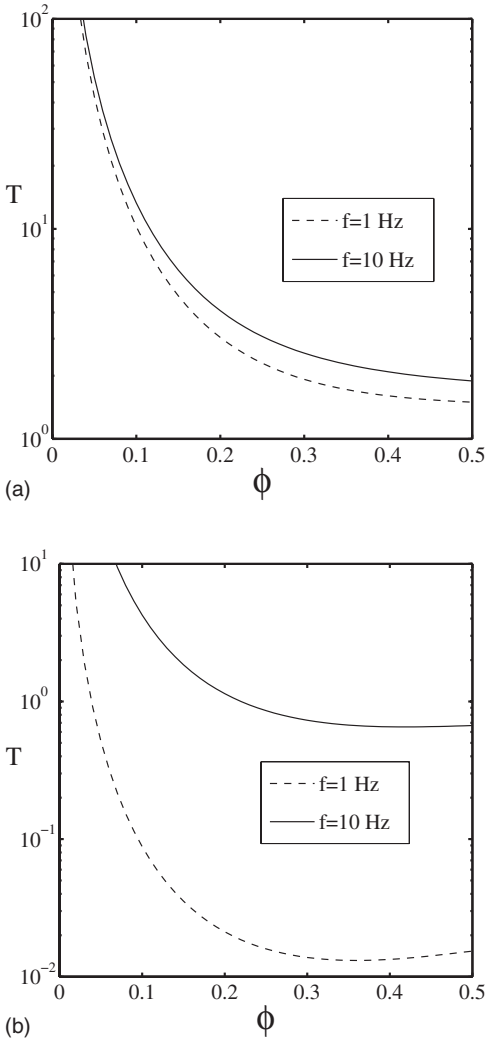

FIG. 2. Variation of the granular temperature T with particle volume fraction for (a) air ($\rho_f=1.165\times10^{-3}$ g/cm^3; $\mu_f=1.86\times10^{-4}$ g/cm/s), and (b) water ($\rho_f=1.0$ g/cm^3; $\mu_f=8.0\times10^{-3}$ g/cm/s), at different shaking frequencies with $A/d=2$. For air, the Stokes numbers are St=46.9 (1 Hz) and 469 (10 Hz); for water, St=1.09 (1 Hz) and 10.9 (10 Hz). Material parameters are $e=0.9$, $d=1.0$ mm, and $\rho_p=2.5$ g/cm^3.

To obtain an expression for the mean velocity of the particles, we integrate the x momentum equation,

$$\rho_p\phi\frac{du}{dt} = F_a + F_d,$$

to yield

$$u(t) = A\omega \cos \omega t - \left(\frac{f_6}{\phi St}\right)\omega \int U_s(t)dt,$$

which boils down to the plate velocity if the drag force is zero (F_d=0). As mentioned before, in the present modeling approach we need to specify the slippage velocity, which is time periodic, $U_s(t)=U\cos \omega t$, where the magnitude of the slippage velocity U is unknown. Therefore, the mean velocity of the suspension is

$$\frac{u(t)}{d\omega} = \left(\frac{A}{d}\right)\cos \omega t - \left(\frac{R_d(\phi)}{St}\right)\left(\frac{U}{d\omega}\right)\sin \omega t, \tag{30}$$

where $R_d(\phi)$ is the drag function, given by Eq. (13).

C. Nondimensional scales

We use the following reference scales for nondimensionalization:

$$L_R = d, \quad t_R = \omega^{-1}, \quad U_R = L_R/t_R = d\omega, \quad T_R = U_R^2. \tag{31}$$

The dimensionless forms of the stress tensor Σ, the drag force $\mathbf{F}_d$, the granular heat flux $\mathbf{q}$, the bulk energy input E, the inelastic dissipation $\mathcal{D}$, and the viscous dissipation $\mathcal{D}_v$ are given by

$$\Sigma^* = \frac{\Sigma}{\rho_p U_R^2} = [p^* - \zeta^*(\nabla^* \cdot \mathbf{u}^*)]\mathbf{I} - 2\mu^* \mathbf{S}^*,$$

$$\mathbf{F}_d^* = \frac{\mathbf{F}_d}{\rho_p U_R^2/L_R} = \frac{1}{\mathrm{St}}(\mathbf{u}_f^* - \mathbf{u}^*)f_6,$$

$$\mathbf{q}^* = \frac{\mathbf{q}}{\rho_p U_R^3} = -\kappa^* \nabla^* T^*,$$

$$E_s^* = \frac{E_s}{\rho_p U_R^3/L_R} = f_7\sqrt{T^*},$$

$$E_h^* = \frac{E_h}{\rho_p U_R^3/L_R} = \frac{1}{\mathrm{St}^2}\frac{U^{*2}}{\sqrt{T^*}}f_{7h},$$

$$\mathcal{D}^* = \frac{\mathcal{D}}{\rho_p U_R^3/L_R} = f_5 T^{*3/2},$$

$$\mathcal{D}_v^* = \frac{\mathcal{D}_v}{\rho_p U_R^3/L_R} = \frac{1}{\mathrm{St}}f_{5v}T^*,$$

and the dimensionless expressions for the pressure, shear viscosity, bulk viscosity, and thermal conductivity are

$$p^* = \frac{p}{\rho_p U_R^2} = f_1 T^*, \quad \mu^* = \frac{\mu}{\rho_p L_R U_R} = f_2\sqrt{T^*},$$

$$\zeta^* = \frac{\zeta}{\rho_p L_R U_R} = f_3\sqrt{T^*}, \quad \kappa^* = \frac{\kappa}{\rho_p L_R U_R} = f_4\sqrt{T^*},$$

respectively. In the following, the asterisks on dimensionless quantities are dropped for simplicity.

IV. LINEAR STABILITY: FLOQUET ANALYSIS

For the linear stability analysis, each of the dynamical variables is decomposed into a base state (i.e., the mean flow, denoted by a superscript 0) and a small-amplitude perturbation (denoted by a prime) as

$$\phi(x,y,t) = \phi^0 + \phi'(x,y,t),$$

$$\mathbf{u}(x,y,t) = \mathbf{u}^0 + \mathbf{u}'(x,y,t),$$

$$T(x,y,t) = T^0 + T'(x,y,t),$$

and the governing equations are linearized about the mean flow, by retaining terms which are linear in the perturbation variables and their derivatives. This results in a set of linear partial differential equations

$$\frac{\partial \mathbf{X}'}{\partial t} = \mathcal{Q}\mathbf{X}', \tag{32}$$

where $\mathbf{X}'(x,y,t)=(\phi',\mathbf{u}',T')$ represents the vector of state variables, and $\mathcal{Q}$ is the associated linear partial differential operator that depends on the mean flow and the driving parameters as detailed in the Appendix.

The stability operator $\mathcal{Q}(t)$ is *time dependent*, but *translationally invariant* in x and y (the latter being a consequence of our assumption that the suspension is of infinite extent in both x and y directions). The translation invariance of $\mathcal{Q}$ allows us to seek a normal mode solution for the perturbation variables,

$$[\phi',u',v',T'](x,y,t) = [\hat{\phi},\hat{u},\hat{v},\hat{T}](t)e^{i(k_x x + k_y y)}. \tag{33}$$

where k_x and k_y are the wave numbers for the x and y directions, respectively. Substituting this ansatz into the linear perturbation equations in the Appendix, we obtain a set of ordinary differential equations

$$\frac{d\hat{X}}{dt} = \mathcal{L}(t)\hat{X}, \tag{34}$$

with $\mathcal{L}(t)=\mathcal{L}(t+2\pi)$ being a time-periodic matrix. The stability matrix $\mathcal{L}(t)$ can be decomposed into time-independent and time-dependent parts:

$$\mathcal{L}(t) = \mathcal{L}_0 + \mathcal{L}_1(t), \tag{35}$$

where the time periodicity of $\mathcal{L}_1(t)=\mathcal{L}_1(t+2\pi)$ arises from the convective terms in each equation, and the drag and acceleration terms (F_d' and F_a') in the x momentum equation.

Since the stability matrix $\mathcal{L}(t)$ is time periodic, we use Floquet theory [24,25] to ascertain the instability or stability of the flow. More specifically, we need to determine the Floquet exponents s_j (j=1,2,3,4) of $\mathcal{L}(t)$ using the fundamental solution matrix [25,26] of Eq. (34) which is calculated numerically [26]. The instability criteria are as follows: (i) if the real part of any Floquet exponent [say, Re(s_j)] is positive (negative), then the flow is unstable (stable); (ii) if there is a Floquet exponent Re(s_j)=0 with multiplicity greater than 1, then the flow is unstable. For details on Floquet theory, the reader is referred to Coddington and Levinson [25].

V. RESULTS AND DISCUSSION

A. Disturbances with $k_x=0$: Channel modes

Here we consider disturbances for which there is no variation along the driving direction, i.e., $\partial/\partial x(.)=0$. This corresponds to disturbances with modulations along the y direction (i.e., orthogonal to the driving direction), and such disturbances can aptly be called "channel" modes since they lead to channelization in density (i.e., alternate layers of high- and low-density bands along the y direction) in an otherwise uniform system. For this case, the linearized disturbance equations are

$$\frac{\partial \phi'}{\partial t} = -\phi^0 \frac{\partial v'}{\partial y}, \tag{36}$$

$$\phi^0 \frac{\partial u'}{\partial t} = \mu^0 \frac{\partial^2 u'}{\partial y^2} + F^0_{d\phi}\phi' + F^0_{a\phi}\phi', \tag{37}$$

$$\phi^0 \frac{\partial v'}{\partial t} = -p^0_\phi \frac{\partial \phi'}{\partial y} - p^0_T \frac{\partial T'}{\partial y} + (2\mu^0 + \lambda^0)\frac{\partial^2 v'}{\partial y^2}, \tag{38}$$

$$\phi^0 \frac{\partial T'}{\partial t} = \kappa^0 \nabla^2 T' - p^0 \frac{\partial v'}{\partial y} + (E^0_\phi - \mathcal{D}^0_\phi - \mathcal{D}^0_{v\phi})\phi' + (E^0_T - \mathcal{D}^0_T - \mathcal{D}^0_{vT})T'. \tag{39}$$

Note that the time periodicity due to convective terms vanishes for $k_x=0$, but the perturbation equations remain time periodic due to the drag and acceleration terms in the x momentum equation. For all results below, the slippage velocity is taken to be a constant, $U/d\omega=1.0$, and the qualitative nature of our results remains the same with a different numerical value of the slippage velocity.

A set of phase diagrams in the (ϕ,k_y) plane is shown in Fig. 3 for three different oscillation amplitudes A/d. The oscillation frequency is set to $f=1$ Hz, with other parameters as in Fig. 2(a) and the interstitial fluid being air. In each panel, the contours of positive growth rate of the most unstable mode $[s_r^l=\sup_j \mathrm{Re}(s_j)>0]$ are shown, along with the neutral stability contour (i.e., the one with zero growth rate, $s_r^l=0$) that demarcates the regions of stable and unstable flows. For $A/d=2$ in Fig. 3(a), it is observed that the flow is unstable only at low volume fractions for a range of transverse wave number k_y. Note that the instability is *stationary* in nature since the corresponding phase speed is zero (not shown). In Fig. 3(b), the neutral contour for $A/d=2$ has been superimposed (denoted by the thick solid line) on the phase diagram for $A/d=10$. Comparing the two neutral contours for $A/d=2$ and 10, we find that the size of the unstable zone has decreased substantially with increasing A/d. With a further increase in A/d to 50 [Fig. 3(c)], however, the size of the unstable zone remains relatively unaffected, but the growth rate increases. The variations of the growth rate of the most unstable mode (s_r^l) with transverse wave number k_y are shown in Fig. 4 for different A/d at a particle volume fraction $\phi=0.1$; other parameters are as in Fig. 3. It is observed that the flow is unstable for a range of k_y for each A/d; increasing the value of A/d from 10 to 50 decreases the range of unstable wave numbers marginally, but the maximum growth rate increases by about a factor of 5.

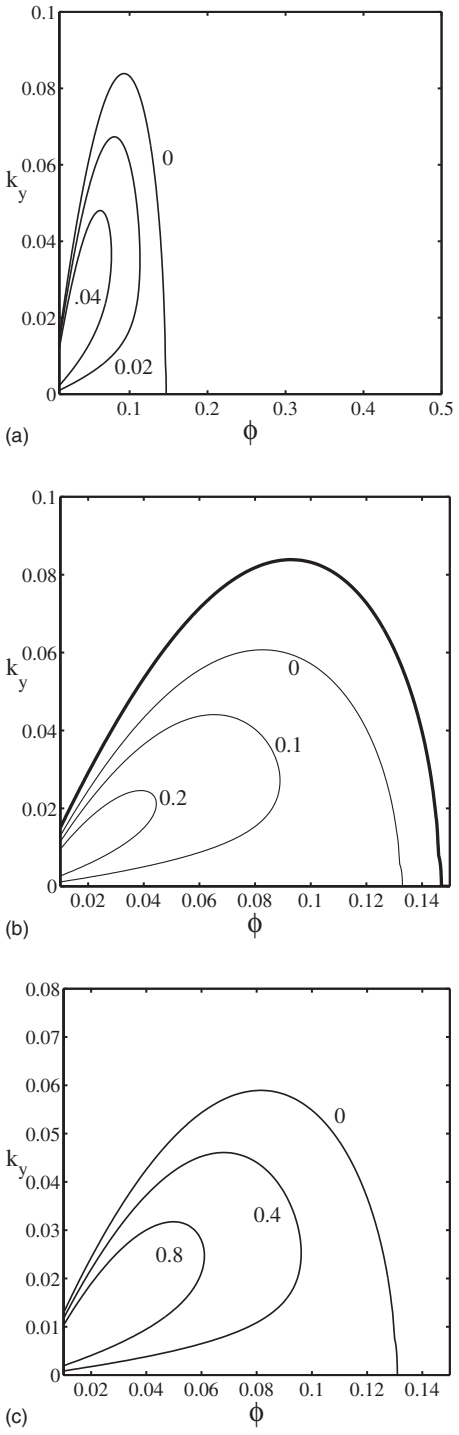

FIG. 3. Effect of driving amplitude A/d on the phase diagram in the (ϕ,k_y) plane for $k_x=0$ at $f=1$ Hz. $A/d=$ (a) 2; (b) 10; (c) 50. In each panel, the contours of positive growth rates are displayed along with the neutral contour (zero growth rate). Thick solid line in (b) represents the neutral contour for $A/d=2$. Material parameters are as in Fig. 2(a) and the interstitial fluid is air.

The effect of oscillation frequency on the observed instability is shown in Fig. 5(a). For this plot, $f=10$ Hz, with other parameters as in Fig. 3(a); the thick line in Fig. 5(a)

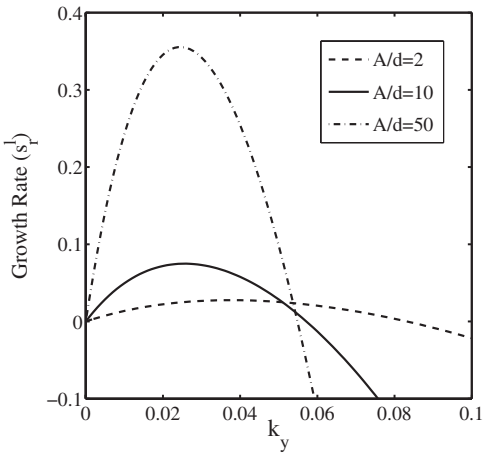

FIG. 4. Effect of driving amplitude A/d on the variation of the growth rate of the most unstable mode with transverse wave number k_y for $k_x=0$, $f=1$ Hz, and $\phi=0.1$. Other parameters are as in Fig. 3.

denotes the neutral contour for $f=1$ Hz. As in the case of increasing A/d, the size of the unstable zone in the (ϕ,k_y) plane decreases with increasing f; with further increase in f to 50 Hz (not shown), the unstable zone remains the same size approximately. For all cases, the instability is stationary. The variations of the growth rate of the most unstable mode with transverse wave number k_y are shown in Fig. 5(b) for $f=1$, 10, and 50 Hz at a particle volume fraction $\phi=0.1$. Recall that the reference time scale for nondimensionalization is $\omega^{-1} \propto f^{-1}$. Therefore, the instability growth rate increases with increasing shaking frequency f as is evident in Fig. 5(b).

To summarize, the oscillatory suspension admits a stationary instability if the particle volume fraction is below some critical value ($\phi=\phi_c \sim 0.15$). This instability corresponds to alternate layers of high- and low-density bands of particles, with the particle bands being aligned parallel to the driving direction (since $k_x=0$). In other words, the predicted instability would lead to channel formation (channelization) along the driving direction, and hence we call it the channel-mode instability.

B. Disturbances with $k_x \neq 0$: Oblique modes

Here we present results for oblique disturbances having variations in both x and y directions ($k_x,k_y \neq 0$). A special case with $k_y=0$ will also be discussed for which the particle bands are orthogonal to the driving direction.

The contours of the most unstable growth rates in the (k_x,k_y) plane are shown in Figs. 6(a)–6(d) for four particle volume fractions $\phi=0.05$, 0.1, 0.3, and 0.5, with driving parameters being set to $A/d=2$ and $f=1$ Hz. In Figs. 6(a) and 6(b), it is observed that the flow is unstable for a range of k_x and k_y at long wavelengths. Recall that the flow is unstable to $k_x=0$ modes at $\phi=0.05, 0.1$ [Fig. 3(a)] which is evident in Figs. 6(a) and 6(b), but is stable for $\phi > \phi_c \sim 0.15$. The interesting finding is that the flow can be unstable even for $\phi > \phi_c$ for a range of k_x at $k_y=0$ as seen in Figs. 6(c) and 6(d). With increasing ϕ, the size of the unstable zone in the (k_x,k_y) plane increases marginally [Figs. 6(c) and 6(d)]; the growth rate of the most unstable mode also increases with increasing ϕ as is evident in Fig. 7(a), which displays the variation of the growth rate of the most unstable mode with k_x. From the corresponding phase speed ($c_{\mathrm{ph}}=s_i^l/\sqrt{k_x^2+k_y^2}$, where s_i^l is the imaginary part of the least stable Floquet mode) variations in Fig. 7(b), we find that the observed instabilities are due to *traveling* waves; this conclusion holds for all instabilities with $k_x \neq 0$ (such as in Fig. 6). Note that the phase speeds are, in general, higher for denser flows. For both Figs. 7(a) and 7(b), $k_y=0.02$ and the other parameters are as in Fig. 6(c).

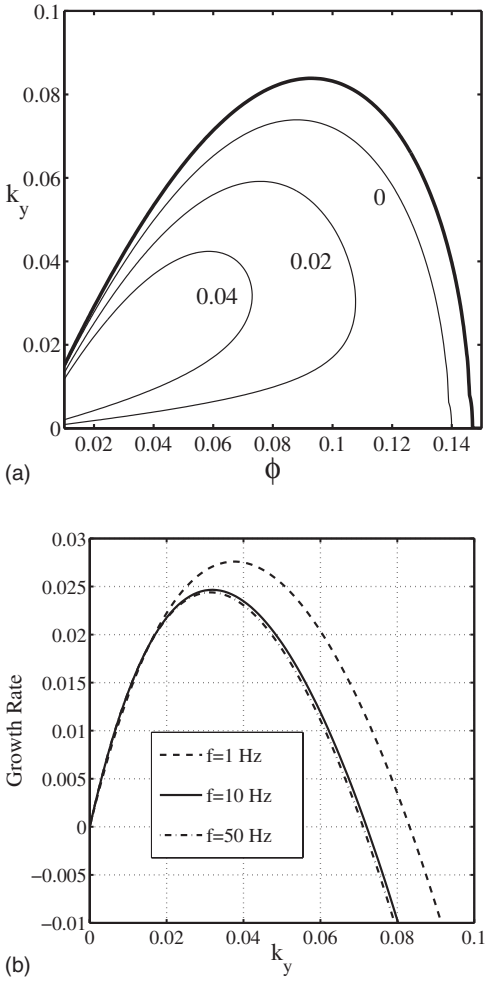

FIG. 5. (a) Phase diagram in the (ϕ,k_y) plane for $k_x=0$ and $A/d=2$ at $f=10$ Hz; the thick solid line represents the neutral contour for $f=1$ Hz. (b) Effect of driving frequency f on the variation of the growth rate of the most unstable mode with k_y for $k_x=0$ and $A/d=2$ at $\phi=0.1$.

The effects of driving amplitude and frequency on observed instabilities can be ascertained from Figs. 8(a) and 8(b), respectively; for both plots, $\phi=0.3$ and $e=0.9$. For Fig. 8(a), the frequency is set to $f=1$ Hz and the amplitude is varied, while for Fig. 8(b) the amplitude is $A/d=2$ and the frequency is varied. For both cases, the size of the unstable zone in the (k_x,k_y) plane shrinks and approaches zero with increasing driving strength. Therefore, the traveling instabilities with $k_x \neq 0$ will disappear at high-amplitude and high-

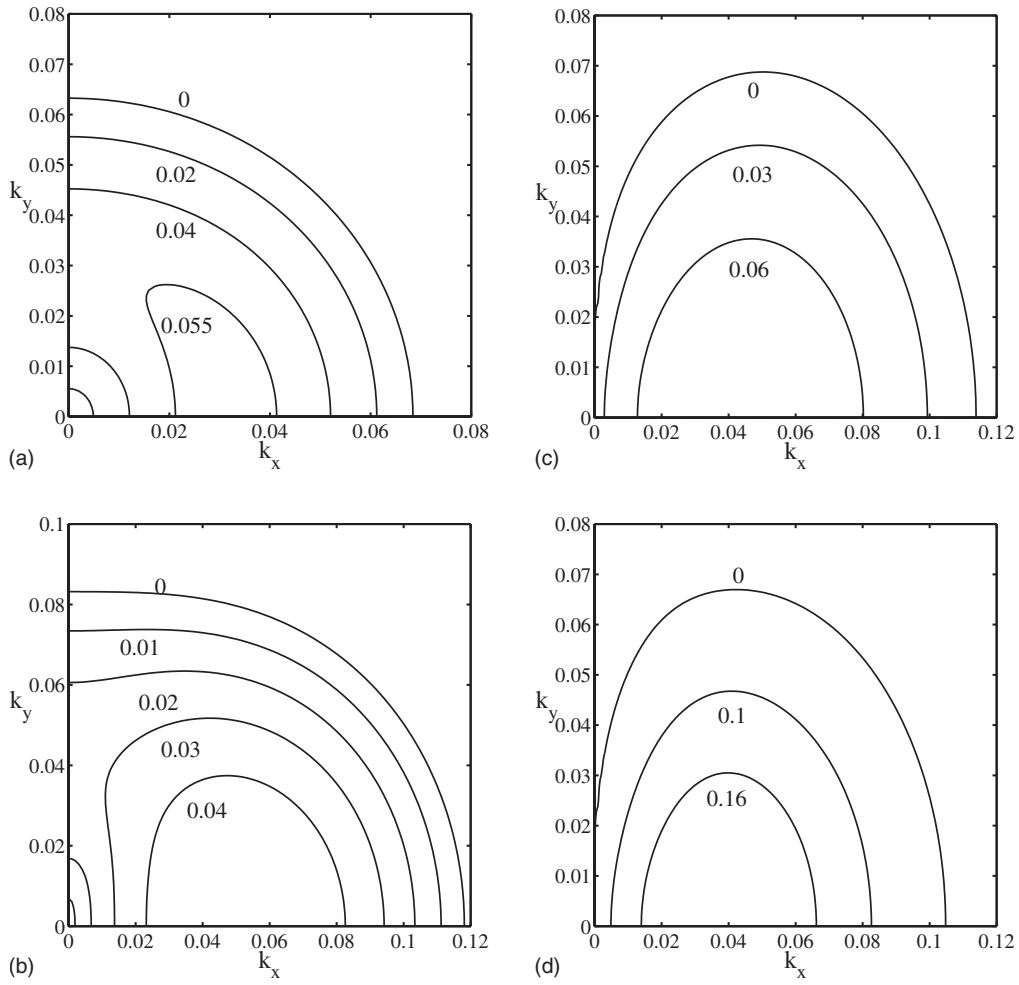

FIG. 6. Phase diagrams in the (k_x,k_y) plane for $A/d=2$ and $f=1$ Hz. $\phi=$ (a) 0.05; (b) 0.1; (c) 0.3; (d) 0.5. Other parameters are as in Fig. 3 and the interstitial fluid is air. In each panel, the contours of positive growth rates are displayed along with the neutral contour (zero growth rate).

frequency oscillations. This is in contrast to the channel-mode instability ($k_x=0$ and $k_y\neq 0$, $\phi<\phi_c\sim 0.15$) which becomes stronger for high-amplitude and high-frequency oscillations.

It may be noted that, for modes with $k_x\neq 0$ and $k_y=0$, the disturbances have variations only along the x direction, and hence such modes are responsible for the formation of particle bands, orthogonal to the driving direction; for nonzero values of both k_x and k_y, the particle banding is *oblique* to the driving direction. The orthogonal particle bands are reminiscent of the ripples (i.e., peaks and valleys of particle density along the driving direction) in a sand bed under an oscillatory driving force.

C. Factors responsible for instability

Since there are many control parameters in the present problem, here we carry out a parametric study to isolate factors that are responsible for the predicted instabilities.

Figure 9(a) shows the phase diagrams in the (ϕ,k_y) plane for two restitution coefficients $e=0.7$ and 1, with parameter values as in Fig. 3(a). For a comparison, the neutral contour for $e=0.9$ is also superimposed, denoted by the thick solid line. It is seen that the suspension remains unstable (shaded region) even in the elastic limit $e=1$; decreasing the value of e increases the size of the unstable zone in the (ϕ,k_y) plane and the growth rates are also larger. These overall observations hold also for instabilities with $k_x\neq 0$ modes as is evident in Fig. 9(b). We can conclude that the inelastic dissipation is not necessary for the onset of these instabilities; however, the strength of instabilities increases with increasing inelasticity. The last effect mirrors a similar observation on instabilities in dry granular shear flows [26–28].

The effects of viscous dissipation on observed instabilities are shown in Figs. 10(a) and 10(b). The shaded zone in each panel, for which the viscous dissipation is set to zero, is unstable which should be compared with the corresponding neutral contour (thick line) for nonzero viscous dissipation. It is clear that the inclusion of viscous dissipation makes the flow unstable for a larger range of parameters. On the whole, the effects of viscous dissipation on these instabilities mirror that of collisional dissipation.

Lastly, we probe the effects of the drag force. The onset of the channel-mode instability ($k_x=0$) is not influenced by the perturbation drag force (F_d') which was verified by setting the drag force to zero in the stability equations; the pertur-

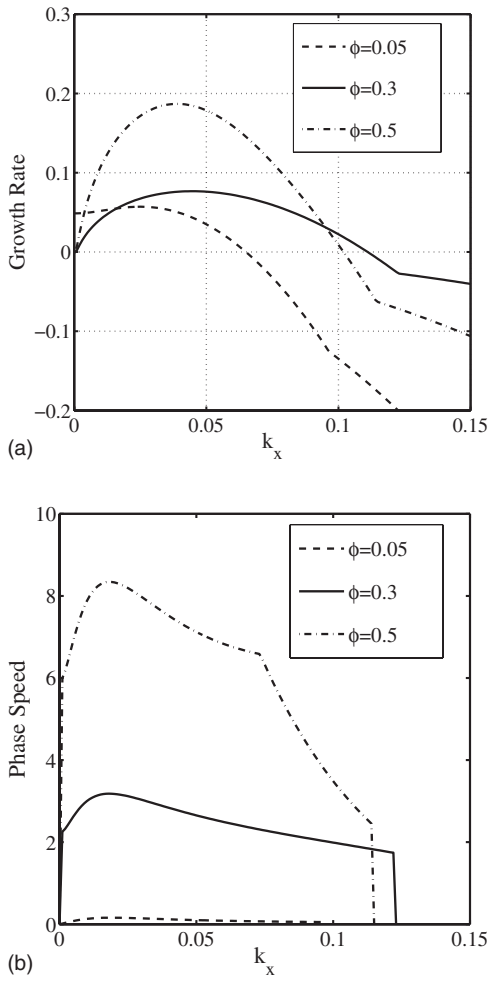

FIG. 7. Variations of the (a) growth rate and (b) phase speed of the most unstable mode with k_x for k_y=0.02 at different ϕ. Other parameters are as in Fig. 6(c).

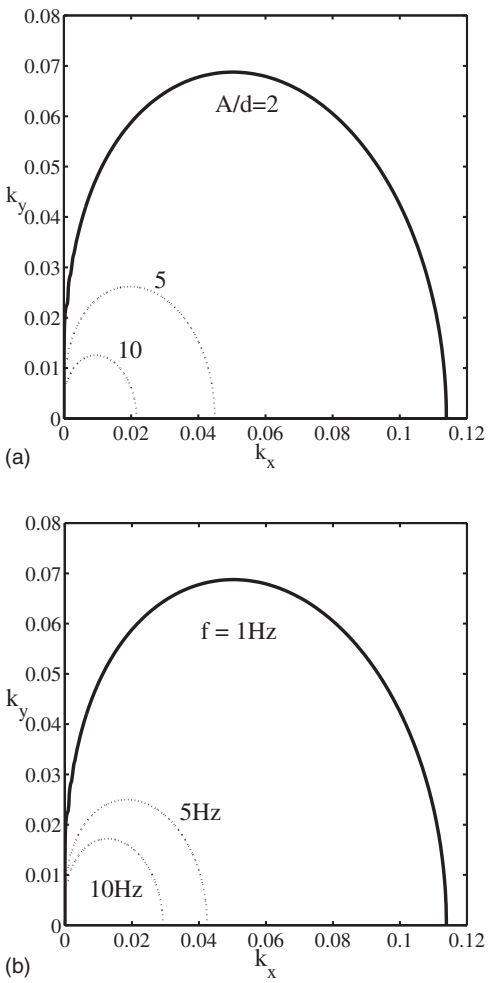

FIG. 8. Effects of driving parameters on phase diagrams in the (k_x,k_y) plane for ϕ=0.3. Only neutral contours are shown: (a) A/d=2 (solid), 5 (dot-dashed), 10 (dotted) with f=1 Hz; (b) f =1 Hz (solid), 5 Hz (dot-dashed), 10 Hz (dotted) with A/d=2. Other parameters are as in Fig. 6(c).

bation acceleration force (F'_a) also does not influence this instability. This can be proved analytically: in the absence of F'_d and F'_a, the x momentum equation (37) gets decoupled from the other three stability equations. For this case, the streamwise velocity perturbation decays as

$$u'(t) = u'(0)\exp(-tk_y^2\mu^0/\phi^0) = u'(0)\exp(-t/\tau_u), \quad (40)$$

with a decay rate $\tau_u^{-1}=(\mu^0 k_y^2/\phi^0)$; hence the observed instability arises due to the coupling among perturbations in density (ϕ'), transverse velocity (v'), and granular temperature (T'). It is clear that the drag force does not influence the channel-mode instability. In contrast, however, the traveling-wave instabilities $(k_x \neq 0)$ owe their existence to the drag force. This is shown in Fig. 11, with parameter values as in Fig. 6(c). The size of the instability zone in the (k_x,k_y) plane diminishes with decreasing magnitude of the drag force, and the flow becomes stable when the drag force is set to zero. Since the drag force is linearly proportional to the slippage velocity [$F_d \propto U$, Eq. (10)], the above conclusions are directly tied to the slippage velocity too. Therefore, the slippage velocity (and hence the drag force) between the particle phase and the fluid is responsible for the emergence of traveling-wave oblique $(k_x \neq 0)$ instabilities.

VI. SUMMARY AND OUTLOOK

Drawing on analogies with the theories of rapid granular flows [2,16] and rapid suspensions [17,18], we have outlined an effective continuum model for a particulate suspension. The balance equations for the particle phase have been augmented by certain interaction terms for the fluid phase, leaving aside the balance equations for the fluid phase altogether. The present continuum model is a "higher-order" model since we have an additional balance equation for the fluctuation energy of the particle phase. We considered a monolayer suspension of infinite extent which is driven harmonically in the horizontal plane; the effects of the oscillating plate are taken into account in the governing equations in a mean-field manner. The mean flow of this oscillatory suspension is characterized by a time-dependent granular temperature, having no spatial gradient; this unsteady temperature relaxes to a

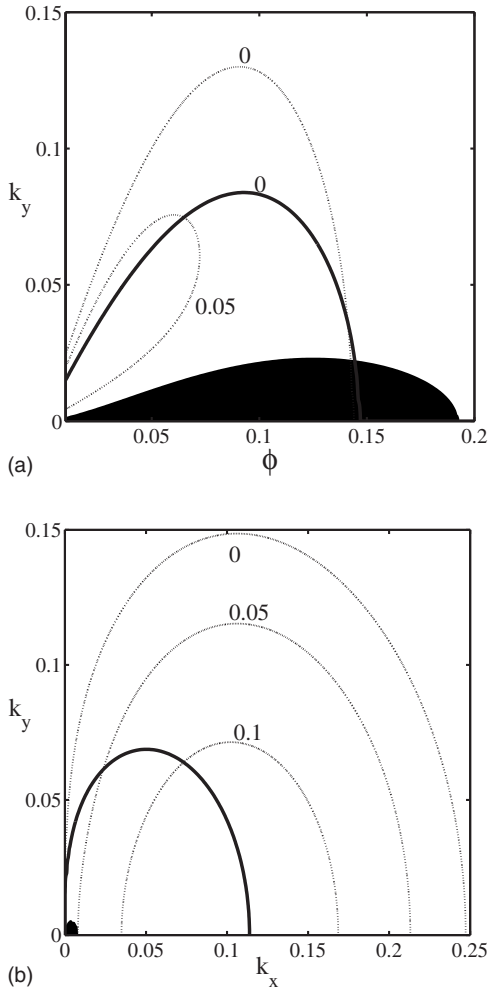

FIG. 9. (a) Effect of restitution coefficient on the phase diagrams in the (ϕ, k_y) plane: parameters as in Fig. 3(a), except for $e=0.7$ for dotted contours and $e=1$ for the shaded zone. (b) Effect of restitution coefficient on the phase diagrams in the (k_x, k_y) plane: parameters as in Fig. 6(c), except for $e=0.7$ for dotted contours and $e=1$ for the shaded zone. The thick line in each panel represents the neutral contour for $e=0.9$.

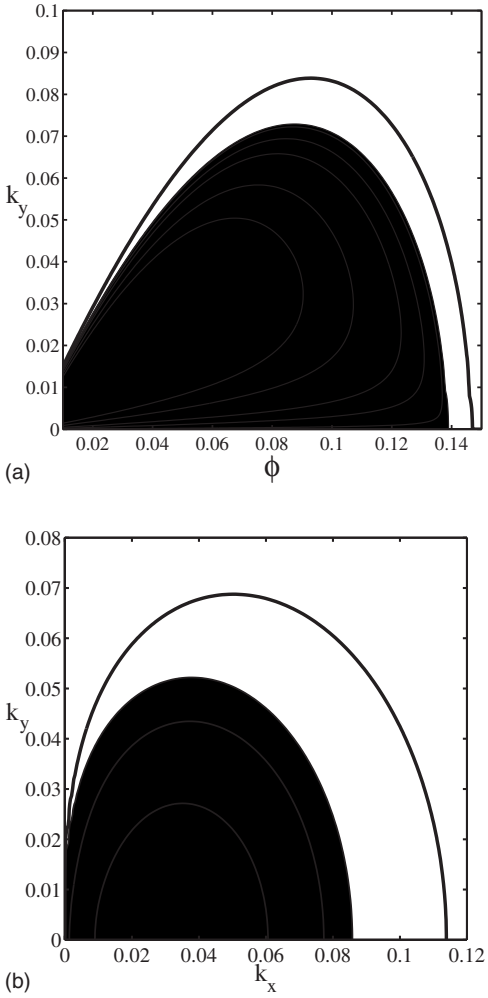

FIG. 10. (a) Effect of viscous dissipation on the phase diagrams in the (ϕ, k_y) plane. Parameters as in Fig. 3(a), except that the viscous dissipation term $(\mathcal{D}_v)$ is zero, for which the flow is unstable in the shaded zone. (b) Effect of viscous dissipation on the phase diagrams in the (k_x, k_y) plane. Parameters as in Fig. 6(c), except that the viscous dissipation term $(\mathcal{D}_v)$ is zero, for which the flow is unstable in the shaded zone. The thick line in each panel represents the neutral contour for nonzero viscous dissipation.

steady value in the asymptotic time limit. Increasing the shaking strength increases the granular temperature of the suspension, implying that the suspension is more fluidized. It should be noted that, since our adopted constitutive model is valid at large Stokes' number, our results are more appropriate for a gas-particle suspension.

While there are many linear stability works (see [26–28], and for reviews [2,4]) on particulate flows with *steady* mean flows, the present work is directed toward analyzing instabilities in a *time-dependent* mean flow. Since the base state of our suspension is time periodic, we have used Floquet theory to determine stability characteristics of this flow. Our results indicate that the oscillatory suspension is unstable to modes with $k_x=0$ (i.e., disturbances having no variation along the driving direction) for a range of transverse wave number k_y if the particle volume fraction is below a critical value $(\phi<\phi_c\sim 0.15)$. The disturbances with $k_x=0$ and $k_y \neq 0$ correspond to the banding of particles parallel to the driving direction, leading to channel formation (i.e., alternate layers of high- and low-density particle bands). This channel-mode instability, which is *stationary* in nature, becomes stronger with increasing amplitude and frequency of oscillation.

For general disturbances, we found that the flow is unstable even at higher particle volume fractions to *traveling-wave* disturbances with $k_y=0$ and $k_x\neq 0$ or a combination of k_x and k_y (oblique disturbance). These traveling-wave instabilities correspond to band formation perpendicular to the driving direction $(k_y=0$ and $k_x\neq 0)$ or at an oblique angle to the driving direction $(k_x, k_y\neq 0)$; they disappear at high-amplitude and high-frequency oscillations which is in contrast to the channel-mode instability.

The present work clearly underscores the important role played by the interstitial fluid on pattern formation in a model oscillatory suspension. While the stationary channel-mode $(k_x=0)$ instability requires both particle-particle and/or fluid-particle interaction terms $(\mathcal{D}$ and $\mathcal{D}_v)$ in the granular

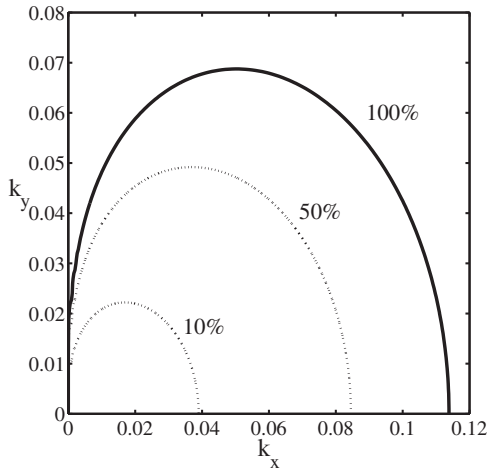

FIG. 11. Effect of drag force F_d on the neutral contour in the (k_x,k_y) plane: F_d (solid), $0.5F_d$ (dotted), and $0.1F_d$ (dot-dashed). Parameters as in Fig. 6(c).

energy balance equation, the traveling-wave instabilities ($k_x \neq 0$) owe their existence to the fluid-particle drag force (F_d) in the momentum equation. These results could be checked via molecular dynamics simulations of an oscillatory particle-fluid suspension. Such an exercise would help to underline the range of validity of the proposed model.

The inclusion of an additional set of balance equations for the fluid phase would be the next step in the hierarchy of model development. Possible implications of the present stability results for ripple formation under oscillatory flow [29] can then be explored by solving the resultant mathematical problem with appropriate boundary conditions [30]. Nevertheless we believe the problem formulated here provides a suitable starting point to study more complex phenomena associated with pattern formation in driven particle-fluid mixtures.

One limitation of our model is the assumption that the particle-fluid mixture is already in a fluidized state. (This issue is inherent in all theories of rapid granular flows which are the starting point of our model [2].) Consequently, our model is unable to predict any lower threshold on driving parameters (A/d and f) beyond which the predicted instabilities would appear. The existence of a lower threshold has been observed in laboratory experiments [9] on the oscillatory flow over a sandy layer, which is, however, different from our uniformly oscillating suspension. Nevertheless, the above possible shortcoming of our model can be rectified in two ways. First, we could assume that the state of uniform fluidization occurs when the driving parameters (A/d and f) exceed some threshold value, and hence the energy source term (20) will vanish if $A\omega$ is small enough [compared to L/τ_r, say, which translates into a Stokes number $\mathrm{St}=(L/A)$, where L is some length scale]. Second, we could use a Bingham-type constitutive model for the stress tensor of the particle phase. These important issues, along with numerical and experimental verification of predicted instabilities, will be taken up in future studies.

ACKNOWLEDGMENTS

This work was supported by the Max Planck Society, Germany via a collaborative project between the MPI-Bremen and the JNCASR under "Max-Planck Partner Group for Topography Formation" (Grant No. MPI/MA/4190), located at JNCASR Bangalore, India.

APPENDIX: LINEARIZED PERTURBATION EQUATIONS

The linearized mass, momentum, and energy balance equations are

$$\frac{\partial \phi'}{\partial t} + u^0(t)\frac{\partial \phi'}{\partial x} = -\phi^0\frac{\partial u'}{\partial x} - \phi^0\frac{\partial v'}{\partial y}, \tag{A1}$$

$$\phi^0\left(\frac{\partial}{\partial t} + u^0(t)\frac{\partial}{\partial x}\right)u' = -p_\phi\frac{\partial \phi'}{\partial x} - p_T\frac{\partial T'}{\partial x} + \left((2\mu^0+\lambda^0)\frac{\partial^2}{\partial x^2} + \mu^0\frac{\partial^2}{\partial y^2}\right)u' + (\mu^0+\lambda^0)\frac{\partial^2 v'}{\partial x\,\partial y} + F_a' + F_d', \tag{A2}$$

$$\phi^0\left(\frac{\partial}{\partial t} + u^0(t)\frac{\partial}{\partial x}\right)v' = -p_\phi\frac{\partial \phi'}{\partial y} - p_T\frac{\partial T'}{\partial y} + \left((2\mu^0+\lambda^0)\frac{\partial^2}{\partial y^2} + \mu^0\frac{\partial^2}{\partial x^2}\right)v' + (\mu^0+\lambda^0)\frac{\partial^2 u'}{\partial x\,\partial y}, \tag{A3}$$

$$\phi^0\left(\frac{\partial}{\partial t} + u^0(t)\frac{\partial}{\partial x}\right)T' = \kappa^0\nabla^2 T' - p^0\left(\frac{\partial u'}{\partial x} + \frac{\partial v'}{\partial y}\right) + (E_\phi^0 - \mathcal{D}_\phi^0 - \mathcal{D}_{v\phi}^0)\phi' + (E_T^0 - \mathcal{D}_T^0 - \mathcal{D}_{vT}^0)T'. \tag{A4}$$

The linear perturbation in the drag term is given by

$$\mathbf{F}_d' = \left(\frac{d\mathbf{F}_d}{d\phi}\right)_{\phi^0,U_s^0}\phi' \equiv \mathbf{F}_{d\phi}^0\phi' \quad \text{with} \quad \mathbf{F}_{d\phi}^0 = \mathrm{St}^{-1}f_{6\phi}^0 U\cos t, \tag{A5}$$

and the linearized acceleration force term is

$$\mathbf{F}_a' = \mathbf{F}_{a\phi}^0\phi' \quad \text{with} \quad \mathbf{F}_{a\phi}^0 = -\left(\frac{A}{d}\right)\sin t. \tag{A6}$$

Both these terms are time periodic (with a period 2π) and so is the base state mean velocity:

$$u^0(t) = \left(\frac{A}{d}\right)\cos t - \left(\frac{R_d(\phi)}{St}\right)U\sin t. \tag{A7}$$

[1] H. M. Jaeger, S. R. Nagel, and R. P. Behringer, Rev. Mod. Phys. **68**, 1259 (1996).; H. J. Herrmann, J.-P. Hovi, and S. Luding, *Physics of Dry Granular Media* (Kluwer Academic, Dordrecht, 1998).
[2] I. Goldhirsch, Annu. Rev. Fluid Mech. **35**, 267 (2003); L. Kadanoff, Rev. Mod. Phys. **71**, 435 (1999).
[3] T. Shinbrot, N. H. Duong, L. Kwan, and M. M. Alverez, Proc. Natl. Acad. Sci. U.S.A. **101**, 8542 (2004).
[4] I. S. Aranson and L. S. Tsimring, Rev. Mod. Phys. **78**, 641 (2006).
[5] R. A. Bagnold, Proc. R. Soc. London, Ser. A **187**, 1 (1946).
[6] R. A. Bagnold, Proc. R. Soc. London, Ser. A **332**, 473 (1973).
[7] J. F. Kennedy, Annu. Rev. Fluid Mech. **1**, 147 (1969); F. Engelund and J. Fredsoe, *ibid.* **14**, 13 (1982).
[8] G. Sauermann, K. Kroy, and H. J. Herrmann, Phys. Rev. E **64**, 031305 (2001); K. Kroy, G. Sauermann, and H. J. Herrmann, Phys. Rev. Lett. **88**, 054301 (2002).
[9] K. J. Richards, J. Fluid Mech. **99**, 597 (1980).
[10] K. H. Andersen, M. L. Chabanol, and M. van Hecke, Phys. Rev. E **63**, 066308 (2001).
[11] C. Faraci and E. Foti, Phys. Fluids **13**, 1624 (2001).
[12] F. Bundgaard, C. Ellegaard, K. Scheibye-Knudsen, T. Bohr, and T. Sams, Phys. Rev. E **70**, 066207 (2004).
[13] T. Hara, C. C. Mei, and K. T. Shum, Phys. Fluids **4**, 1373 (1992).
[14] R. Jackson, *The Dynamics of Fluidized Particles* (Cambridge University Press, Cambridge, U.K., 2000); D. Gidaspow, *Multiphase Flows and Fluidization* (Academic, San Diego, 1994).
[15] D. Lohse, R. Bergmann, R. Mikkelsen, C. Zeilstra, D. vanderMeer, M. Versluis, K. vanderWeele, M. vanderHoef, and H. Kuipers, Phys. Rev. Lett. **93**, 198003 (2004); G. Caballero, R. Bergmann, D. van der Meer, A. Prosperetti, and D. Lohse, *ibid.* **99**, 018001 (2007); J. L. Vinningland, O. Johnsen, E. G. Flekkoy, R. Toussaint, and K. J. Maloy, *ibid.* **99**, 048001 (2007); X. Cheng, G. Varas, D. Citron, H. M. Jaeger, and S. R. Nagel, *ibid.* **99**, 188001 (2007).
[16] C. K. K. Lun, S. B. Savage, D. J. Jeffrey, and C. Chepurniy, J. Fluid Mech. **140**, 223 (1984).
[17] Y. A. Buyevich, Chem. Eng. Sci. **49**, 1217 (1994).
[18] A. S. Sangani, G. Mo, H.-K. Tsao, and D. L. Koch, J. Fluid Mech. **313**, 309 (1996).
[19] B. J. Glasser, S. Sundaresan, and I. G. Kevrekidis, Phys. Rev. Lett. **81**, 1849 (1998).
[20] D. Ma and G. Ahmadi, J. Chem. Phys. **84**, 3449 (1986).
[21] M. A. van der Hoef, R. Beetstra, and J. A. M. Kuipers, J. Fluid Mech. **528**, 233 (2005).
[22] H. C. Brinkman, Appl. Sci. Res., Sect. A **1**, 27 (1949).
[23] S. Kim and W. B. Russel, J. Fluid Mech. **154**, 269 (1985); A. J. C. Ladd, J. Chem. Phys. **93**, 3484 (1990).
[24] S. H. Davis, Annu. Rev. Fluid Mech. **8**, 57 (1976).
[25] E. A. Coddington and N. Levinson, *Theory of Ordinary Differential Equations* (McGraw-Hill, New York, 1955).
[26] M. Alam and P. R. Nott, J. Fluid Mech. **343**, 267 (1997).
[27] S. B. Savage, J. Fluid Mech. **241**, 109 (1992).
[28] B. Gayen and M. Alam, J. Fluid Mech. **567**, 195 (2006).
[29] F. Charru and J. Hinch, J. Fluid Mech. **550**, 123 (2006).
[30] J. A. Ochoa-Tapia and S. Whitaker, Int. J. Heat Mass Transfer **38**, 2635 (1995).